SM: Collective filament wrapping and nested spiral formation in active polydisperse systems

Caterina Landi,[1] Giulia Janzen,[2] Francesco Sciortino,[3] John Russo,[3] Chantal Valeriani,[1] and Daniel A. Matoz-Fernandez[2]

[1] *Department of Structure of Matter, Thermal Physics, and Electronics, Complutense University of Madrid, Madrid, 28040, Spain.*
[2] *Department of Theoretical Physics, Complutense University of Madrid, Madrid, 28040, Spain*
[3] *Department of Physics, Sapienza Universitá di Roma, 00185 Rome, Italy.*

(Dated: December 26, 2025)

I. MODEL

Bonded interactions comprise a stretching and bending contribution, $\phi_B = \phi_{bond} + \phi_{bend}$. The stretching contribution is modeled by the Tether potential [1], which has an attractive part

$$\phi_{bond}^{attr}(r_{ij}) = \begin{cases} \dfrac{k_b \exp[1/(l_{c_0} - r_{ij})]}{l_{\max} - r_{ij}}, & r_{ij} > l_{c_0} \\ 0, & r_{ij} \leq l_{c_0}, \end{cases} \tag{S1}$$

and a repulsive part at short distances

$$\phi_{bond}^{rep}(r_{ij}) = \begin{cases} \dfrac{k_b \exp[1/(r_{ij} - l_{c_1})]}{r_{ij} - l_{\min}}, & r_{ij} < l_{c_1} \\ 0, & r_{ij} \geq l_{c_1}, \end{cases} \tag{S2}$$

where r_{ij} is the particle-particle distance, k_b the bond stiffness, l_{c_0} the cutoff length of the attractive potential, $l_{\max}$ the maximum bond length, $l_{\min}$ the minimum bond length, and l_{c_1} the cutoff length of the repulsive potential. The bond reference length b is related with the parameters introduced above according to SI TableI. Note that, in our regime of small bond-length fluctuations, the choice between the Tether and FENE potentials has negligible impact on system behavior [2]. The bending contribution is modeled by the harmonic angle potential [3]

$$\phi_{bend}(\theta) = \kappa(\theta - \theta_0)^2, \tag{S3}$$

where κ denotes the bending rigidity, θ is the angle formed by neighboring bonds, and θ_0 is the rest angle. Non-bonded interactions, ϕ_{NB}, account for steric repulsion and are modeled with the Weeks-Chandler-Anderson (WCA) potential [4]

$$\phi_{NB}(r_{ij}) = \begin{cases} 4\epsilon \left[\left(\dfrac{\sigma}{r_{ij}} \right)^{12} - \left(\dfrac{\sigma}{r_{ij}} \right)^{6} \right] + \bar{\phi}(r_{ij}), & r_{ij} < 2^{1/6}\sigma \\ 0, & r_{ij} > 2^{1/6}\sigma, \end{cases} \tag{S4}$$

where r_{ij} represents the particle-particle distance, ϵ the depth of the potential well, σ the characteristic length scale of the interaction (commonly interpreted as the bead diameter) and $\bar{\phi}(r_{ij})$ a shifting term ensuring that the potential and its derivatives vanish smoothly. All simulation parameters are listed in SI Table I, organized into two sections: interaction parameters (introduced above) and other parameters (introduced in the main text).

One simulation parameter not reported in SI Table I is the bending rigidity κ, which varies with the filament length L. We highlight that κ defines the bending rigidity in a discrete model and is related to the continuum bending rigidity $\tilde{\kappa}$ through the relation $\tilde{\kappa} = 2b\kappa$, leading to the thermal persistence length being defined as $\xi_p = \tilde{\kappa}/k_BT = 2b\kappa/k_BT$. [3]. Solving $\xi_p/L = 2b\kappa/(Lk_BT)$ for κ and substituting $L \approx b(N_b - 1)$, we obtain

$$\kappa = \frac{\xi_p}{L} \frac{k_BT(N_b - 1)}{2}. \tag{1}$$

Equation (1) shows that, being the persistent ratio ξ_p/L fixed for all filaments, κ increases linearly with the number of beads N_b. Values of κ per N_b corresponding to the persistent ratio $\xi_p/L = 1.3$ are reported in SI Table II.

SI Table I. Simulation parameters expressed in the reduced unit system: length in σ, energy in ε, and time in $\tau = \sqrt{m\sigma^2/\varepsilon}$.

Interaction parameters	
Bond stiffness	$k_b = 10$
Bond reference length	$b = 0.86$
Maximum bond length	$l_{\max} = 1.55\,b$
Minimum bond length	$l_{\min} = 0.2\,b$
Tether cutoffs	$l_{c_0} = 0.75\,b\ , \quad l_{c_1} = 0.1\,b$
Rest angle	$\theta_0 = \pi$
Other parameters	
Number of particles	$N = 5 \times 10^4$
Packing fraction	$\rho = 0.3$
Damping coefficient	$\gamma = 1.0$
Thermal energy	$k_BT = 0.1$
Péclet number	$Pe \in 10 \times \{0.5, 1, 3, 5, 7, 9, 11, 13, 16, 19\}$
Persistence ratio	$\xi_p/L = 1.3$
Integration time step	$\delta t = \begin{cases} 10^{-3}, & Pe < 160 \\ 5 \times 10^{-4}, & Pe \geq 160 \end{cases}$
Relaxation time	8×10^4 time steps
Averaging	100 configurations sampled every 500 time steps
Integrator scheme	BAOAB [5]
Simulation package	SAMoS [6]

SI Table II. Bending rigidity κ as a function of the number of beads N_b for $\xi_p/L = 1.3$.

κ	N_b
0.13	3
0.65	11
1.235	20
1.755	28
2.34	37
2.86	45
3.445	54
3.965	62
4.55	71
5.135	80

II. NESTED SPIRALS

We define a nested spiral as a structure in which the centers of mass of all constituent filaments lie within a threshold distance of $\bar{r} = 3.0$. For lower activities ($Pe \leq 10$), where these assemblies tend to be less compact, we relax this criterion to $\bar{r} = 5.0$ to ensure complete inclusion of all filaments. To qualify as a nested spiral, the structure must also exhibit a sufficiently large collective turning number, defined as $\psi_{\text{nested}} = \sum_{i=1}^{N_f} |\psi_i|$, where N_f denotes the number of filaments in the structure. We impose a threshold $\bar{\psi}_{\text{nested}} = 2.0$ to distinguish between disordered clusters and genuinely spiral arrangements. To exclude unwound filaments, we apply length-dependent thresholds $\bar{\psi}$ on the individual turning numbers ψ (see SI Table III). These thresholds increase with filament length, reflecting the potential for more convoluted spirals in longer filaments. Notably, for filaments with $N_b \geq 37$ at high activity ($Pe \geq 110$), we impose a stricter threshold to account for the dichotomy observed in this regime: filaments tend to either be completely unwound or form tightly wound spirals. This behavior arises from a non-monotonic response to activity, where increased propulsion initially promotes spiral compaction but ultimately destabilizes the formed structures, leading to filament uncoiling.

In our analysis, the distance criterion was used only as an initial screening step to identify candidate structures, serving as a practical way to start filtering the configurations before applying more robust criteria. As a second step, we applied the collective turning number criterion, which allowed us to distinguish genuine spiral-like structures from simple aggregates of open chains. This measure was more robust than the turning number of single chains, as it captured the collective organization of the structure as a whole. The turning number of individual filaments was then applied only at the final cleaning stage. The distance thresholds for screening were chosen by visual inspection,

SI Table III. The turning number ψ of a filament with N_b beads must exceed a threshold value $\bar{\psi}$ to be considered part of a nested spiral. No threshold is applied for filaments with $N_b = 3$, as they are too short to exhibit meaningful spiral configurations. To prevent the misidentification of unwound filaments as spiral elements, for $N_b \geq 37$, a higher threshold is imposed when $Pe \geq 110$. In this high-activity regime, medium and long filaments tend to either adopt tightly wound spiral states or become fully unwound, necessitating a stricter criterion.

N_b	$\bar{\psi}$
3	*null*
11	0.1
20	0.4
28	0.5
≥ 37	$\begin{cases} 0.6 & \text{if } Pe < 110 \\ 2.0 & \text{if } Pe \geq 110 \end{cases}$

ensuring that the selected ones reliably captured the relevant structures. Their values were adjusted according to activity: at low Pe, spirals were less compact and thus required a slightly larger threshold to be captured. Using the same larger threshold across all Pe, would have led at high Pe to the inclusion of many medium-length filaments that were not spirals but only passed nearby while exploring space.

To test the robustness of our results with respect to the definition of nested spirals, we vary the activity-dependent distance threshold $\bar{r}$ by $\pm 20\%$, $\pm 40\%$, and $\pm 60\%$. Structural properties of nested spirals are then recalculated for each modified threshold value (see SI Fig. 1). The conclusion of this analysis is that the results reported in the main text are not qualitatively affected by these variations. When the threshold variation increases in absolute value, deviations become more pronounced at lower Péclet numbers. This is consistent with our motivation for using an activity-dependent threshold. Without applying a larger threshold in this regime, the deviations would have been even more significant. Overall, however, the robustness of the results is confirmed. For completeness, we execute the same sensitivity test for the collective turning number threshold $\bar{\psi}$ (see SI Fig. 2). Same conclusions can be drawn.

Furthermore, to test the robustness of the results presented in the phase diagram of Fig. 4 of the main text with respect to the definition of nested spirals, we varied the distance and collective turning number thresholds, for a small ($\xi_p/L = 0.8$, see SI Fig. 3) and a big ($\xi_p/L = 3.05$, see SI Fig. 4) persistent ratio value, by previous amounts: $\pm 20\%$, $\pm 40\%$, and $\pm 60\%$. Results reported in the main text are not qualitatively affected by these variations. When the threshold variation increases in absolute value, deviations become more pronounced where the number of number of nested spirals is high.

A. Structural properties

The structure of nested spirals varies with activity. With increasing activity, these structures converge toward a state in which they are composed exclusively of two filaments. This behavior (described in more detail in the main text) is quantitatively captured by the probability distribution of number of filaments per nested spiral, $P(N_f)$, illustrated in SI Fig. 5. In the low-activity regime, nested spirals typically consist of two or three filaments. As activity increases, the fraction of two-filament nested spirals rises, while that of three-filament ones decreases. Ultimately, increasing activity drives the system toward a state dominated by two-filament nested spirals.

Further insight into the structural composition of nested spirals is provided by the average filament length, $\bar{l}$, normalized by the length of the longest filament in the system, l_0. This ratio ranges from $\bar{l}/l_0 = 1$, when nested spirals are composed exclusively of filaments of length 80 (the longest), down to $\bar{l}/l_0 = 0.0375$, when they are composed exclusively of filaments of length 30 (the shortest). As shown in SI Fig. 6, this quantity reflects how the characteristic length within nested spirals changes with activity. At low activity, it indicates that nested spirals are primarily composed of long filaments. As activity increases, the average length decreases, consistent with the emergence of nested spirals formed by two filaments of differing length, one long and one short (behavior described in more detail in the main text). At even higher activity, the average length increases, due to the uncoiling of medium filaments, which become dynamically unstable when strongly propelled. In fact, the destabilization of the two-filament nested spirals involving medium-length filaments (rather than long ones) occurs first. Hence, the small increase at high activity can be attributed to the reentrant transition occurring at different activities for different lengths.

To further characterize the morphology of nested spirals, we compute their collective turning number, defined as $\psi_{\text{nested}} = \sum_{i=1}^{N_{\text{nested}}} |\psi_i|$, i.e. the sum of the absolute values of the turning number of the individual filaments within each spiral. As shown in SI Fig. 7, ψ_{nested} exhibits a non-monotonic dependence on activity. It first increases, reflecting

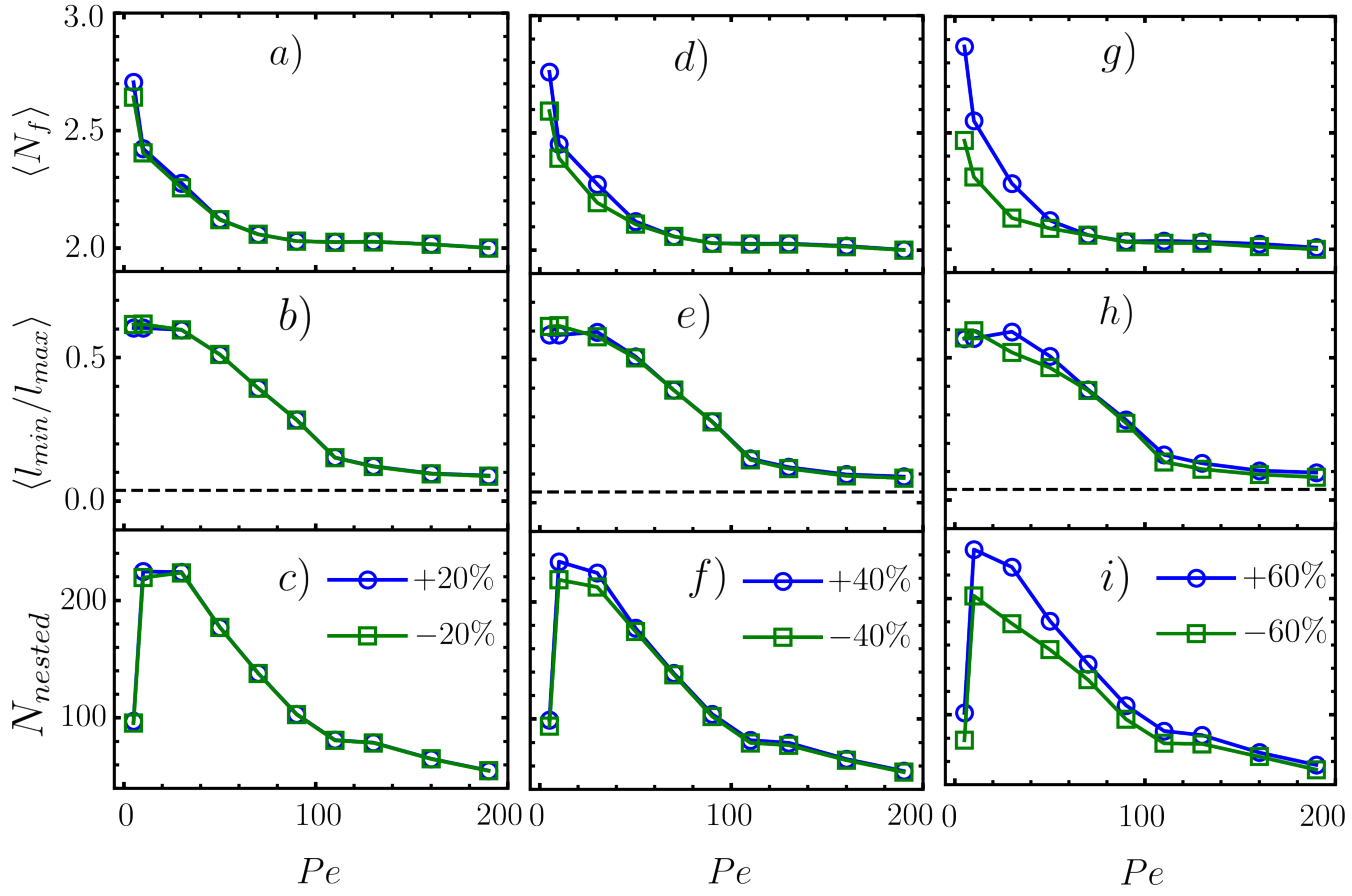

SI Fig. 1. Structural properties of the nested spirals as a function of the Péclet number for different variations of the distance threshold $\bar{r}$: ±20% (a–c), ±40% (d–f), and ±60% (g–i). Green squares indicate a decrease of the threshold, while blue circles indicate an increase. (a, d, g) Average number of filaments per nested spiral, $\langle N_f \rangle$. (b, e, h) Average length ratio of the shortest to the longest filament in each nested spiral, $\langle l_{\mathrm{min}}/l_{\mathrm{max}} \rangle$. (c, f, i) Total number of nested spirals, N_{nested}.

the formation of more compact nested spirals. In the intermediate regime, it decreases as medium-length filaments become unstable and begin to uncoil, weakening the overall spiral structure. For $Pe \geq 110$, the turning number increases again. This second increase is attributed to the contribution of long filaments that form tightly coiled pairs with short filaments before eventually becoming unstable themselves. The non-monotonic behavior of ψ_{nested} thus reflects the dynamic restructuring of nested spirals across activity regimes.

B. Monodisperse case

To assess the role of polydispersity in the emergence of the structural transition, we also simulated a monodisperse system composed of filaments of only one length.

Snapshots of the system at steady state for a high activity level ($Pe = 190$) are shown in SI Fig. 8. The left panel shows the polydisperse system analyzed in the main text, while the right panel displays a monodisperse system composed exclusively of filaments with length $N_b = 54$. In the polydisperse case, filaments of length $N_b = 54$ are shown in blue and all others in gray. In the monodisperse case, each filament is colored differently. In the polydisperse system, several filaments are uncoiled, while in the monodisperse case all filaments form tightly wound spirals, resulting in a gas-like assembly of compact structures.

Snapshots of the system at steady state for a high activity level ($Pe = 50$) are shown in SI Fig. 9. The left panel shows the polydisperse system analyzed in the main text, while the right panel displays a monodisperse system composed exclusively of filaments with length $N_b = 28$. In the polydisperse system, almost all filaments form tightly wound spirals, while in the monodisperse case some spirals still form but also many filaments are uncoiled, resulting in a mostly fluid-like filament system.

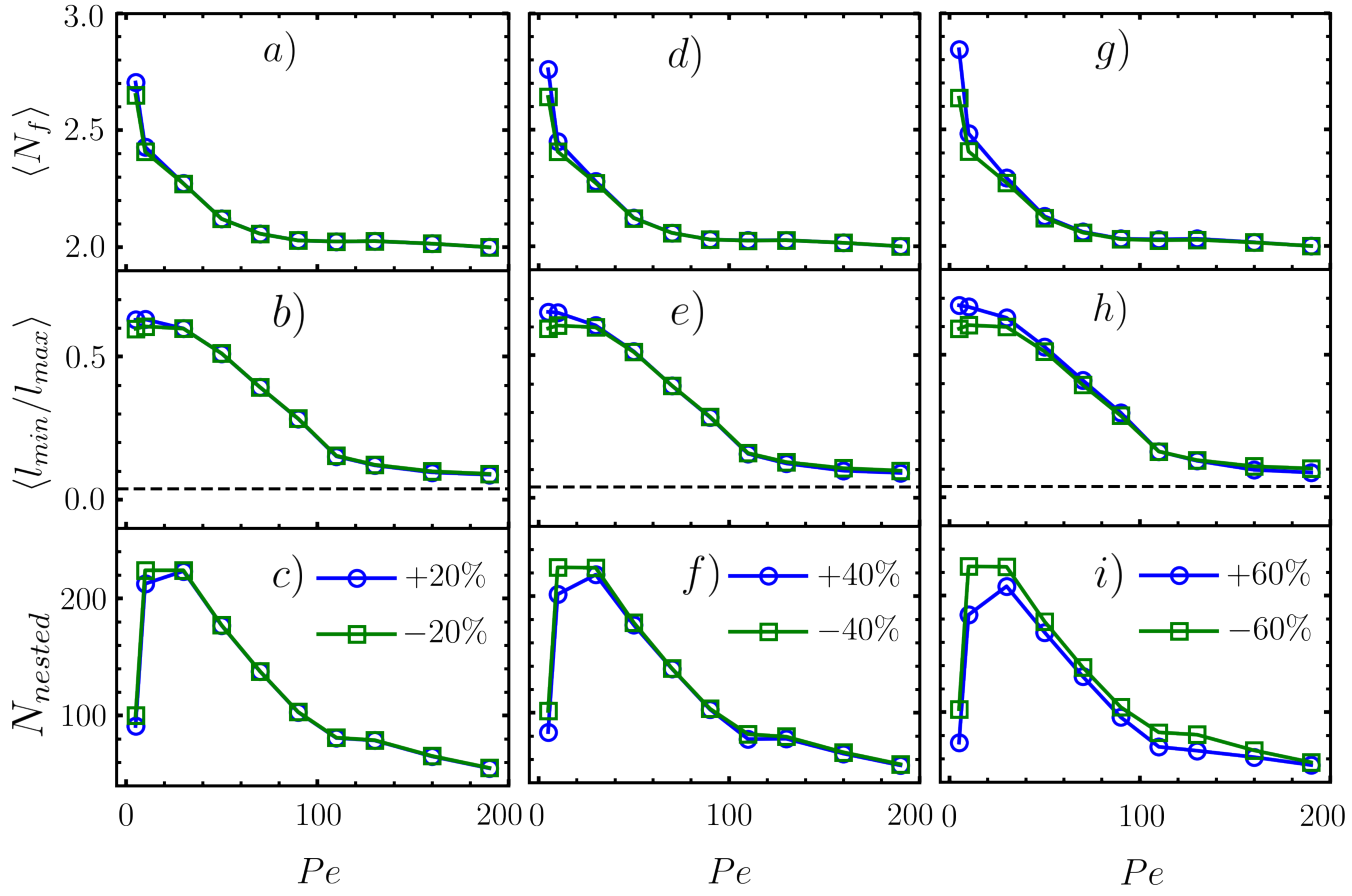

SI Fig. 2. Structural properties of the nested spirals as a function of the Péclet number for different variations of the collective turning number threshold $\bar{\psi}$: ±20% (a–c), ±40% (d–f), and ±60% (g–i). Green squares indicate a decrease of the threshold, while blue circles indicate an increase. (a, d, g) Average number of filaments per nested spiral, $\langle N_f \rangle$. (b, e, h) Average length ratio of the shortest to the longest filament in each nested spiral, $\langle l_{\min}/l_{\max} \rangle$. (c, f, i) Total number of nested spirals, N_{nested}.

To properly address the qualitative difference between the polydisperse and monodisperse cases, we show the fraction of filaments of length $N_b = 28$ in a spiral configuration in SI Fig. 10. While a reentrant behavior is hinted at in the monodisperse case, the number of filaments forming spirals remains small compared to the total number of filaments, which explains the low average turning number for this filament length (see Fig. 1(b)). Instead, in the polydisperse case, around activities where the peak is centered, we reach a situation in which all filaments are in a spiral configuration.
To capture the role of polydispersity in the spiral formation of this filament length, SI Fig. 11 reports the fraction of filaments in a spiral configuration that belong to a nested spiral. For the polydisperse case, a peak at low Pe indicates that these spirals form because long filaments wrap around shorter ones. As longer filaments tend to become more compact with increasing activity, short filaments tend to be single spirals at higher Pe.

C. Uniform filament length distribution

For completeness, we report in SI Fig. 12 the average turning number $\langle |\psi| \rangle$ as a function of the Péclet number for each filament length N_b present in the system with uniform length distribution analyzed in the main text.

D. Exponentially decaying filament length distribution

To test the robustness of our results, we repeated the analysis using a system with an exponentially decaying filament length distribution, in contrast to the uniform distribution considered in the main text. The exponential distribution

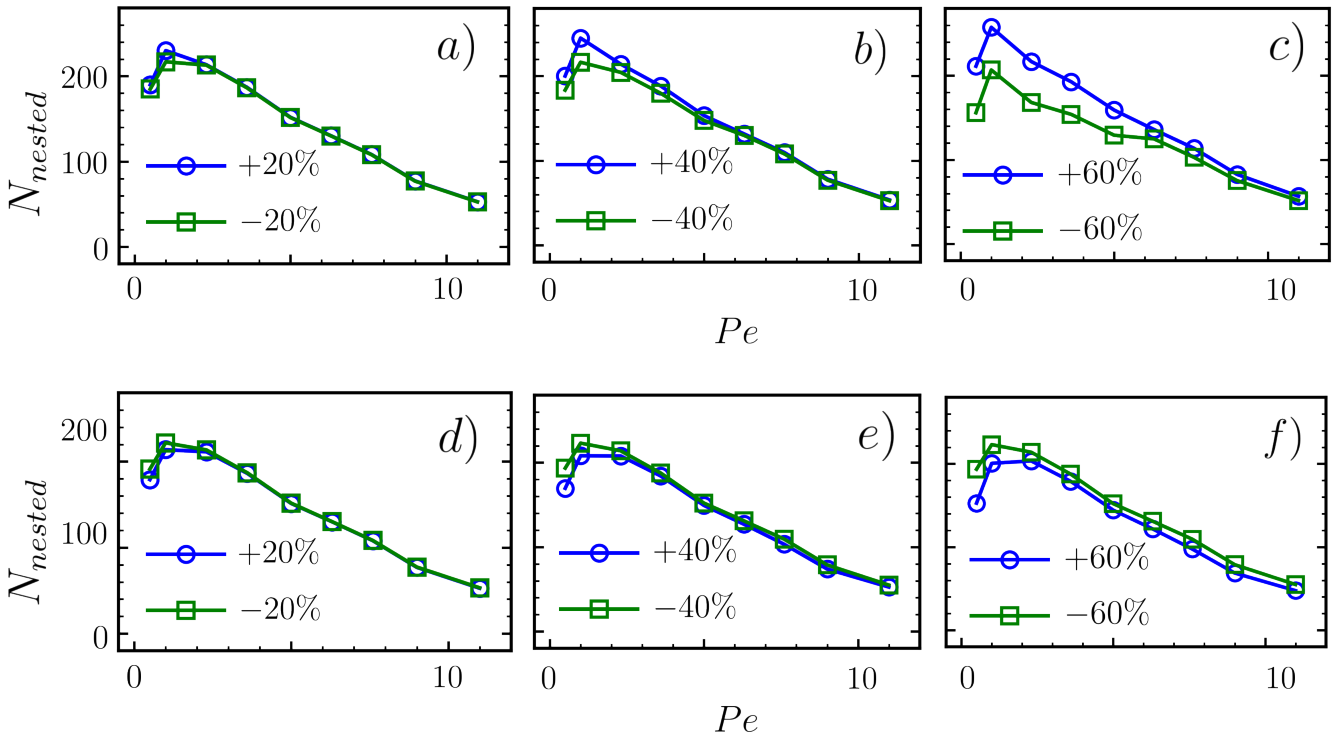

SI Fig. 3. Total number of nested spirals, N_{nested}, as a function of the Péclet number for different variations of the distance threshold $\bar{r}$ (a-c) and collective turning number threshold $\bar{\psi}$ (d-f) at persistent ratio equal to $\xi_p/L = 0.8$. Thresholds are varied by ±20% (a, d), ±40% (b, e), and ±60% (c, f). Green squares indicate a decrease of the threshold, while blue circles indicate an increase.

used is equal to $exp{-}N_b/\tau$ with $\tau = 20$. As shown in the snapshots (SI Fig. 14) and in the measurements of the average turning number (SI Fig. 13) and structural properties (SI Fig. 15), no qualitative differences are observed. The same collective behaviors, including the formation and evolution of nested spirals with activity, persist across both distributions, confirming that our findings do not depend on the specific shape of the filament length distribution.

E. Dynamical Properties

To investigate the dynamical behavior of the system, in the main text we present the self part of the van Hove function, as it directly captures the dynamical heterogeneity of short filaments. As shown there, short filaments display a bimodal displacement distribution, revealing the coexistence of freely motile and trapped configurations. For comparison, in Fig. 16 we also report the mean square displacement (MSD) of the same population of short filaments at two distinct Péclet numbers, $Pe = 10$ and $Pe = 110$. The MSD exhibits the typical short-time ballistic regime (MSD $\sim t^2$) followed by a long-time diffusive regime (MSD $\sim t$), consistent with active polymer dynamics [7]. However, since the MSD averages over all filaments, it completely washes out the dynamical heterogeneity of short filaments: the coexistence of mobile and trapped filaments is no longer visible. For this reason, the van Hove function provides a more suitable observable to capture the dynamics in this regime, whereas the MSD is reported mainly to show the expected average scaling behavior.

We have also evaluated the probability distribution of the normalized lifetime of nested spirals τ_s (see SI Fig. 17). The results indicate that nested spirals are stable within the studied time range. Therefore, the unwinding occurs during the equilibration stage once Pe is increased.

[1] H. Noguchi and G. Gompper, *Phys. Rev. E*, 2005, **72**, 011901.
[2] G. Janzen and D. A. Matoz-Fernandez, *Soft Matter*, 2024, **20**, 6618–6626.

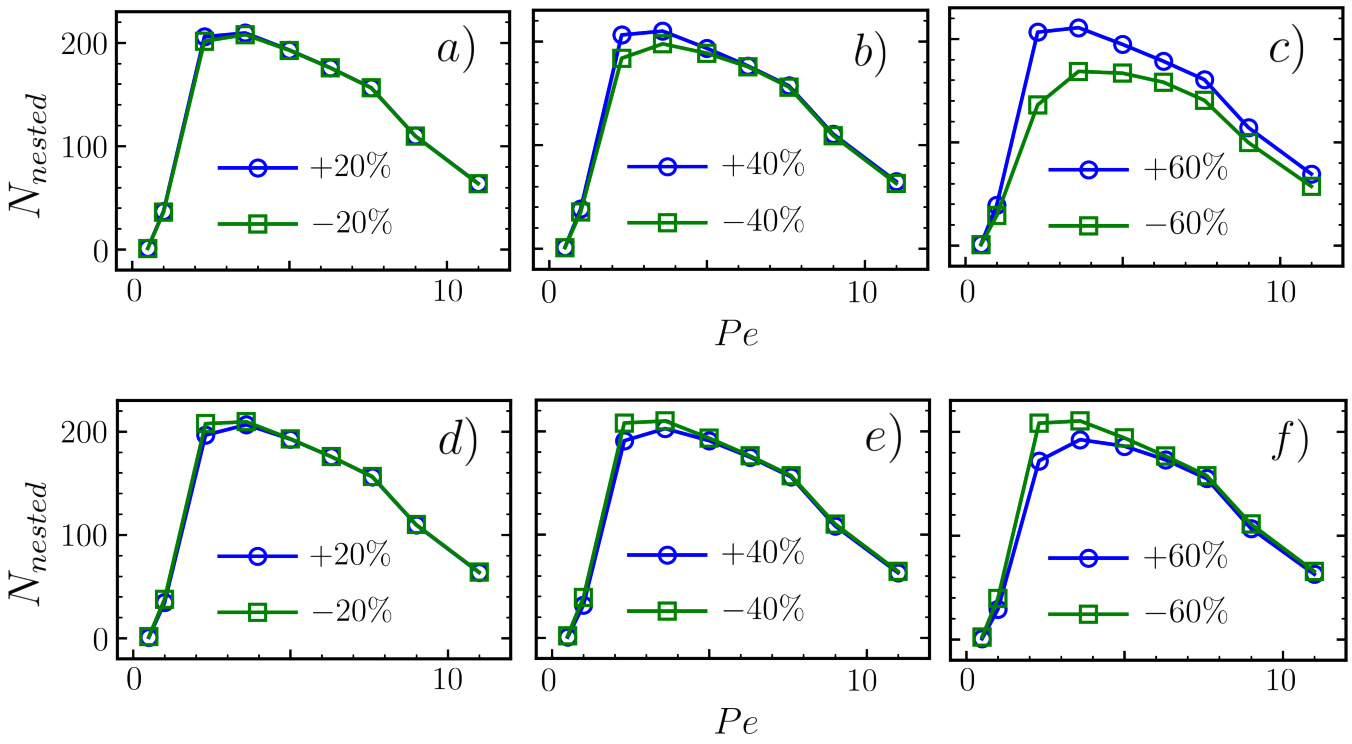

SI Fig. 4. Total number of nested spirals, N_{nested}, as a function of the Péclet number for different variations of the distance threshold $\bar{r}$ (a-c) and collective turning number threshold $\bar{\psi}$ (d-f) at persistent ratio equal to $\xi_p/L = 3.05$. Thresholds are varied by ±20% (a, d), ±40% (b, e), and ±60% (c, f). Green squares indicate a decrease of the threshold, while blue circles indicate an increase.

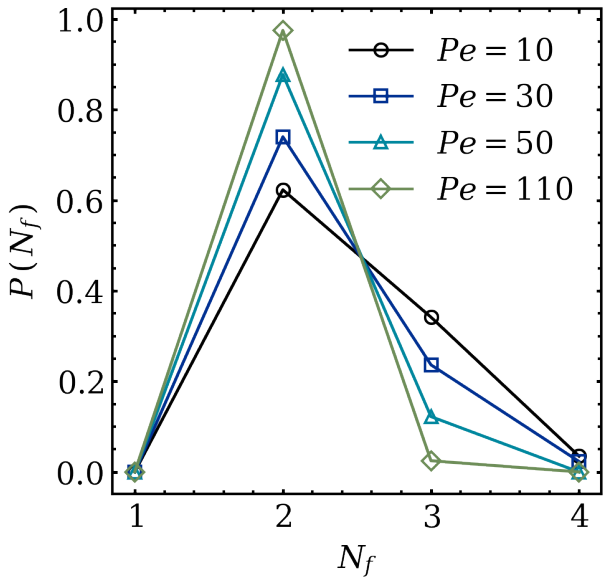

SI Fig. 5. Probability distribution of number of filaments per nested spiral, $P(N_f)$, for different Péclet numbers: black circles for $Pe = 10$, dark blue squares for $Pe = 30$, light blue triangles for $Pe = 50$, and green diamonds for $Pe = 110$. At $Pe = 10$, nested spirals are composed of either two or three filaments. As Pe increases, the fraction of two-filament nested spirals grows, while that of three-filament ones diminishes. At $Pe = 110$, all observed nested spirals consist exclusively of two filaments.

[3] K. R. Prathyusha, S. Henkes and R. Sknepnek, *Physical Review E*, 2018, **97**, 022606.

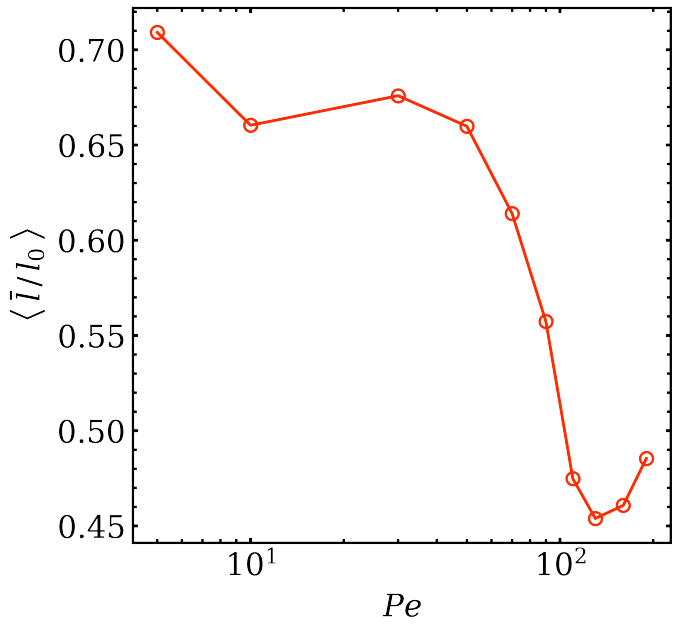

SI Fig. 6. Average length of filaments in a nested spiral normalized by the length of the longest filament in the system, $\langle \bar{l}/l_0 \rangle$. The notation $\langle \dots \rangle$ indicates an ensemble average over all nested spirals. As Pe increases, the average length first decreases ($Pe \leq 110$) and then increases ($Pe > 110$). Both trends are consisted with the structural transition of nested spirals described in the main text: at low Pe, nested spirals consist of more than two filaments of similar length, whereas at higher Pe, they are composed of just two filaments, one long and one short. This figure also highlights that, at small Pe, not only filaments are similar in length, but they are predominately the long ones. The increase occurs when nested spirals consist already exclusively of two filaments. As the medium-length filament are the first to uncoil with increasing activity, nested spirals made of these filaments are the first to break apart.

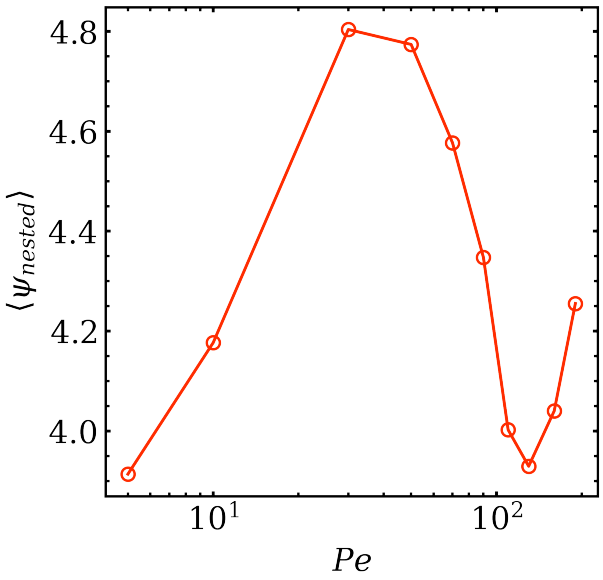

SI Fig. 7. Collective turning number, $\psi_{nested} = \sum_{1=1}^{N_{nested}} |\psi_i|$, as a function of the Péclet number. First, it increases ($Pe \leq 50$), then it decreases ($50 < Pe < 110$), and then it increases again ($Pe \geq 110$). It increases as the nested spirals becomes more and more compact, it decreases as the medium-length filaments start to unwind and break the multi-filament nested spirals. It increases again when nested spirals made of only two filaments (one long and one short) begin to break apart.

[4] J. D. Weeks, D. Chandler and H. C. Andersen, *The Journal of chemical physics*, 1971, **54**, 5237–5247.
[5] B. Leimkuhler and C. Matthews, *Molecular Dynamics: With Deterministic and Stochastic Numerical Methods*, Springer

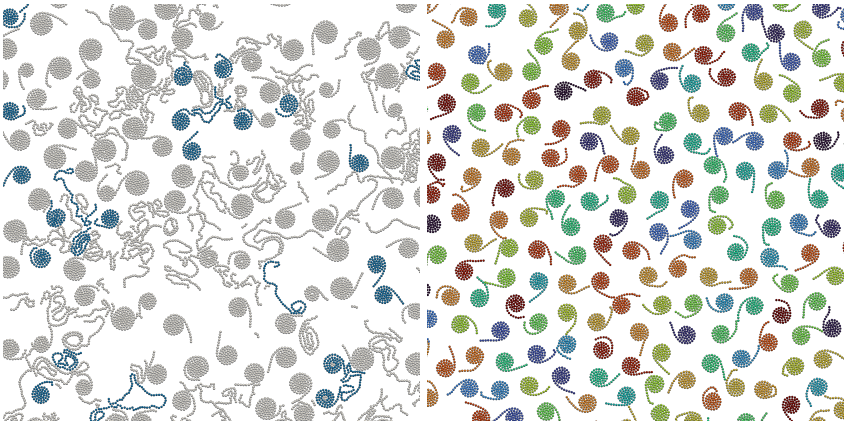

SI Fig. 8. Steady-state snapshots taken at $Pe = 190$: the left panel shows the polydisperse system analyzed in the main text, while the right panel shows a monodisperse system composed exclusively of filaments with length $N_b = 54$. In the left panel, we depict in blue the filaments with $N_b = 54$ and in gray all other filaments. In the right panel, a different color simply indicates a different filament.

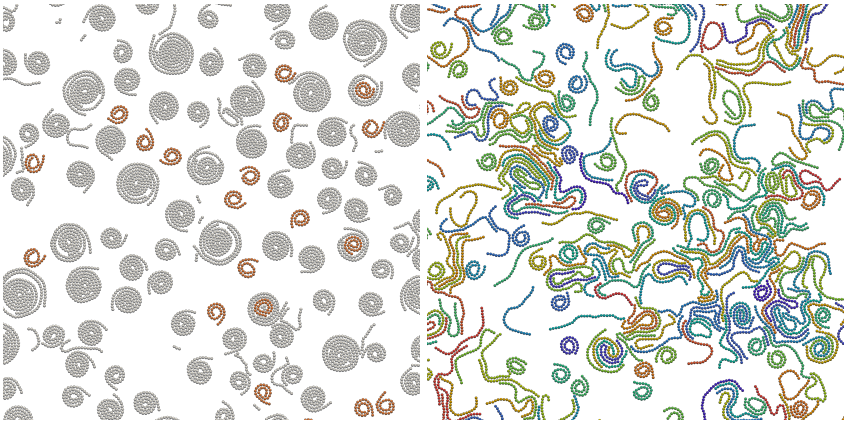

SI Fig. 9. Steady-state snapshots taken at $Pe = 50$: the left panel shows the polydisperse system analyzed in the main text, while the right panel shows a monodisperse system composed exclusively of filaments with length $N_b = 28$. In the left panel, we depict in orange the filaments with $N_b = 28$ and in gray all other filaments. In the right panel, a different color simply indicates a different filament.

International Publishing, 2015.

[6] R. Sknepnek, *SAMoS: Self-propelled Agent-based Models with SAMoS*, `https://github.com/sknepneklab/SAMoS`, 2024, Accessed: 2024-04-29.

[7] O. Duman, R. E. Isele-Holder, J. Elgeti and G. Gompper, *Soft matter*, 2018, **14**, 4483–4494.

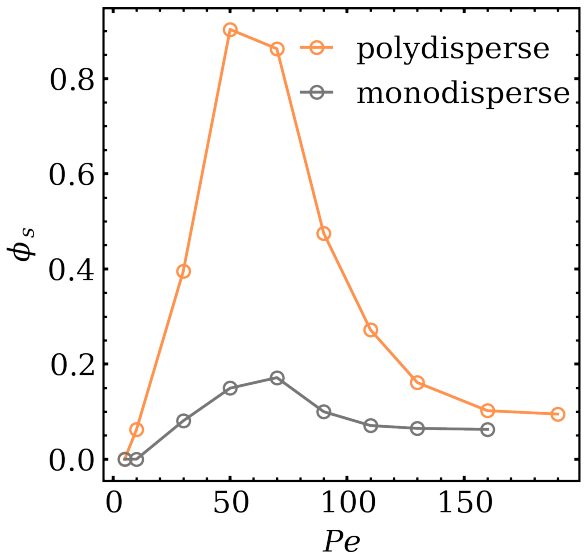

SI Fig. 10. Fraction of filaments of length $N_b = 28$ in a spiral configuration ϕ_s, shown for the polydisperse (orange circles) and monodisperse (gray circles) systems.

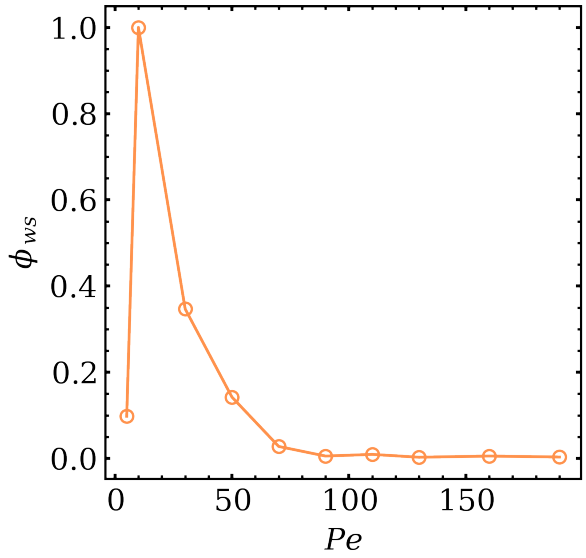

SI Fig. 11. Fraction of filaments in a spiral configuration (length $N_b = 28$) that belong to a nested spiral ϕ_{ws}, shown for the polydisperse system.

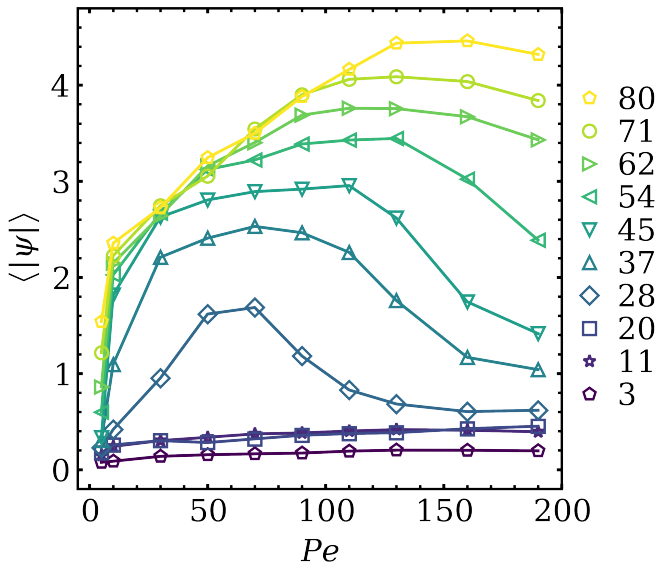

SI Fig. 12. Average turning number, $\langle|\psi|\rangle$, as a function of the Péclet number for the system with an uniform filament length distribution (system studied in the main text). The value of $\langle|\psi|\rangle$ is shown for each filament length N_b present in the system (see legend).

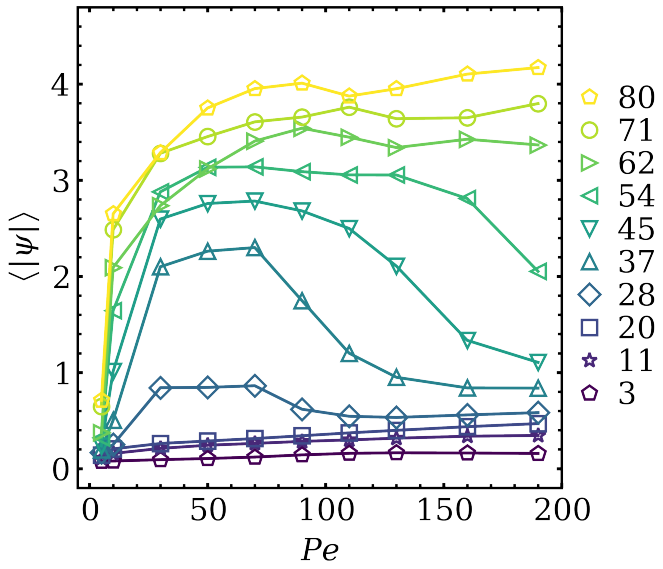

SI Fig. 13. Average turning number, $\langle|\psi|\rangle$, as a function of the Péclet number for the system with an exponentially decaying filament length distribution. The value of $\langle|\psi|\rangle$ is shown for each filament length N_b present in the system (see legend).

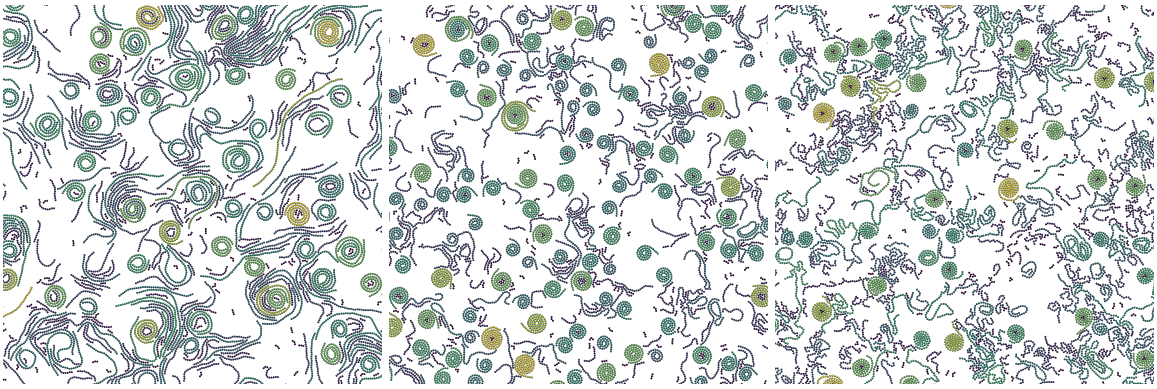

SI Fig. 14. Snapshots of the system with an exponentially decaying filament length distribution at steady-state for a small Péclet number, $Pe = 10$, a medium Péclet number, $Pe = 70$, and a big Péclet number, $Pe = 190$.

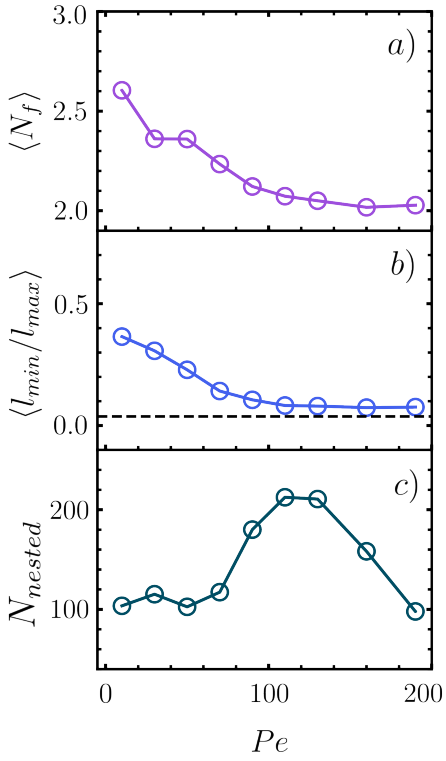

SI Fig. 15. Structural properties of nested spirals as a function of the Péclet number for the system with an exponentially decaying filament length distribution. Panels (a, b) report ensemble-averaged quantities computed over all identified nested spirals. (a) Average number of filaments per nested spiral, $\langle N_f \rangle$. At low Pe, nested spirals typically contain more than two filaments, while at high Pe, they are predominantly composed of filament pairs. (b) Average length ratio of the shortest to the longest filament in each nested spiral, $\langle l_{\min}/l_{\max} \rangle$. The dotted black line at $y = 3/80$ denotes the minimum possible ratio based on the set of filament lengths in the system. At low Pe, filaments within nested spirals tend to be of similar length, while at high Pe, they exhibit pronounced length disparity. (c) Total number of nested spirals, N_{nested}. After a stationary state, this quantity increases at intermediate activity, reaches a peak, and then decreases with further increases in Pe.

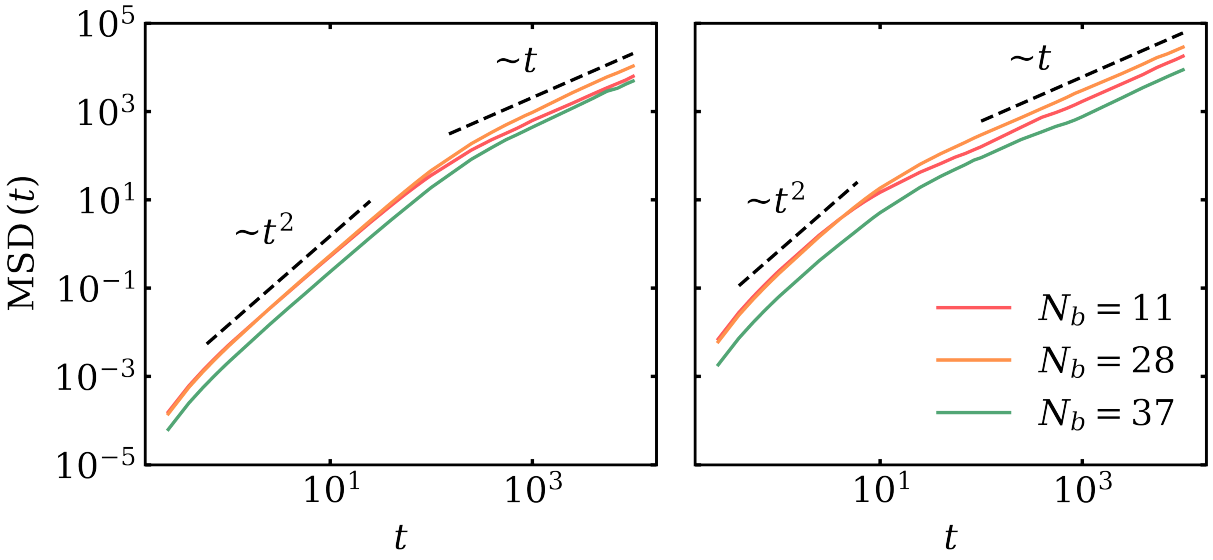

SI Fig. 16. Mean square displacement (MSD) of the center of mass of filaments per different filament length ($N_b = 11, 28$, and 37, see legend) at $Pe = 10$ (left panel) and $Pe = 110$ (right panel). Grey and black dashed lines, proportional to $\sim t^2$ and $\sim t$ respectively (see legend), are shown as visual guides.

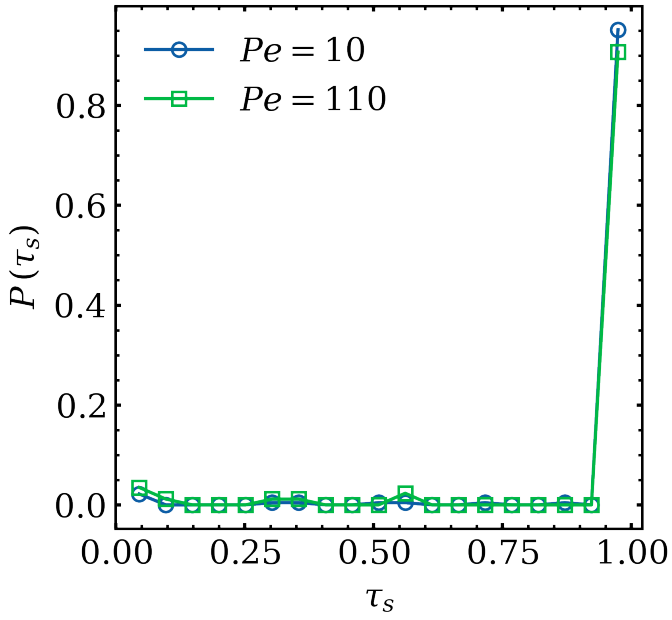

SI Fig. 17. Probability distribution of normalized lifetime of nested spirals τ_s at two different Péclet numbers, $Pe = 10$ (blue circles) and $Pe = 110$ (green squares).